Symmetry breaking effects in epitaxial magnetic thin films: Nonsymmetric reversal and butterfly remanence behavior

David Ecija, Erika Jiménez, Nikolai Mikuszeit,* Nicolás Sacristán, and Julio Camarero†
Departamento de Física de la Materia Condensada and Instituto "Nicolás Cabrera," Universidad Autónoma de Madrid, 28049 Madrid, Spain

Jose María Gallego
Instituto de Ciencia de Materiales de Madrid-CSIC, 28049 Madrid, Spain

Jan Vogel
Institut Néel-CNRS, 38042 Grenoble, France

Rodolfo Miranda
Departamento de Física de la Materia Condensada and Instituto "Nicolás Cabrera," Universidad Autónoma de Madrid, 28049 Madrid, Spain
and Instituto Madrileño de Estudios Avanzados en Nanociencia IMDEA-Nanociencia, Campus Universidad Autónoma de Madrid, 28049 Madrid, Spain

(Received 4 September 2007; published 25 January 2008)

A consistent picture which explains the effects of magnetic anisotropy symmetry breaking on the magnetic properties of epitaxial magnetic thin films is provided, including experimental results in γ'-$Fe_4N(100)$ thin films and numerical simulations. As expected for a thin film with fourfold crystal symmetry, the results show the existence of two easy and two hard magnetization axes. However, in this case, the easy axes are *not orthogonal*, the hard axes are *not equivalent*, the magnetization reversal behavior around the two easy axes is *not symmetric*, and the reversal behaviors of the two hard axes are *not alike*. As a consequence, the polar plot of the remanence displays a *butterfly* shape behavior. These effects depend on additional terms of the magnetic anisotropy. Our results are extended to other symmetry breaking epitaxial magnetic systems.

DOI: 10.1103/PhysRevB.77.024426 PACS number(s): 75.30.Gw, 75.60.Jk, 75.70.−i, 85.70.Kh

I. INTRODUCTION

The advances made during the past decades on materials science and magnetism have made artificial magnetic nanostructures an interesting class of materials from both fundamental and applied points of view.[1] The improved understanding of epitaxial growth processes at the atomic scale has led to the fabrication of custom-designed epitaxial systems, such as ultrathin films, superlattices, or nanostructures.[2] Hysteresis and magnetization reversal investigations are fundamental for the understanding of magnetism on the nanoscale.[3] The reversible vs irreversible magnetization reversal is often manifestation of the symmetry of the system. Artificial epitaxial structures represent hence model systems to study the influence of reduced dimensionality and symmetry on magnetic properties.[4]

Breaking the symmetry of magnetic systems results in additional contributions to the magnetic anisotropy, which could alter both magnetization easy and hard axes and reversal processes. For instance, the origin of the out-of-plane uniaxial magnetic anisotropy observed in some multilayered heterostructures is the orbital moment anisotropy originating from the interfaces.[5] Symmetry breaking at atomic steps or anisotropic lattice relaxation are at the origin of the in-plane uniaxial magnetic anisotropy contribution observed in cubic crystal symmetry systems, in epitaxial magnetic thin films of metals,[6–10] diluted semiconductors,[11–13] as well as oxides.[14] Additional uniaxial anisotropy has also been found in oblique incidence epitaxial and sputtering grown films, as a consequence of the formation of elongated structures oriented perpendicular to the plane of incidence, due to steering during deposition[15] and ripple formation during sputtering,[16] respectively. Moreover, in general, the competition between the cubic and the additional uniaxial anisotropy results in a spin-reorientation transition which depends on intrinsic parameters, such as substrate step density,[6] ferromagnetic thickness[6,7,9,10,14–16] and angle of deposition,[15,16] or extrinsic ones, such as temperature range.[6,11–14]

The purpose of this paper is to give a general picture on the magnetic properties, including both characteristic magnetization axis directions and magnetization reversal processes, of epitaxial magnetic systems with broken symmetry. Vectorial Kerr magnetometry measurements have been performed in well characterized metallic γ'-$Fe_4N(100)$ thin films, in which the fourfold crystal symmetry of the film is broken by a twofold contribution probably originating from stress relaxation. Nonorthogonal easy axes are found, as in epitaxial magnetic semiconductor compounds.[11] Additional features in the magnetization reversal behavior have been also identified. The broken symmetry induces nonsymmetric reversal behavior around the easy axes, different reversal modes at the hard axes, and a "butterfly-shaped" polar plot of the remanence. A simple model, which includes biaxial (fourfold) and uniaxial (twofold) magnetic anisotropy contributions, has been used to address all these features, and is extended to other symmetry breaking epitaxial systems. The anisotropy

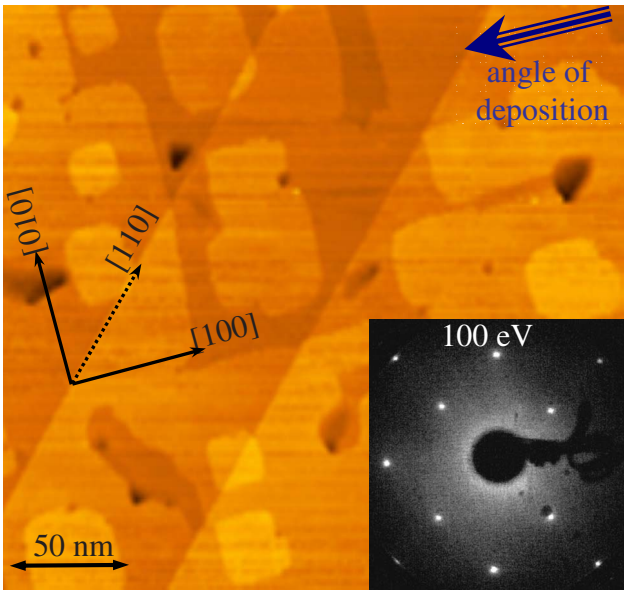

FIG. 1. (Color online) STM image of a 20 ML thick iron nitride film grown on Cu(100). The angle of deposition and the crystallographic directions are indicated. The inset shows the corresponding LEED pattern.

ratio is the key parameter which controls these effects.

The paper is organized as follows. We describe the experimental details in Sec. II. The results and the discussions are presented in Sec. III. We address the question of the origin of the observed unusual behaviors of the magnetization reversal and easy-axis directions on the basis of the anisotropy balance. A detailed description of the model is further reported in the Appendix . The summary is presented in Sec. IV, concluding that the control of the anisotropies is thus required in order to tailor both easy-axis directions and reversal processes in epitaxial magnetic systems.

II. EXPERIMENT

The growth mode and structure of single-phase γ'-$Fe_4N(100)$ films grown at 700 K on Cu(100) have been studied *in situ* from the early stages up to 50 nm thick films by means of room temperature scanning tunneling microscopy (STM), low energy electron diffraction (LEED), and Auger electron spectroscopy.[17] The films are single crystals with sharp interfaces with the substrate, atomically flat and grown layer by layer (see Fig. 1). Besides the expected islands steps, the STM images show the existence of a number of straight, monatomic steps running along the ⟨110⟩ directions and, although they exist in the two orthogonal directions, one of them is always greatly preferred in all the grown films. The origin of the steps is still unclear, but they have been created after the film was grown (since some of them can be seen crossing already formed islands), maybe as a way of relieving the stress in the grown film during the cooling procedure. The films were capped with a 3 nm thick Cu layer to avoid oxidation in air during the magnetic characterization. On flat surfaces, like the one of γ'-$Fe_4N(100)$, this sealing protects several years (in this case at least two) from oxidation.

The magnetic characterization was performed at room temperature by high-resolution vectorial Kerr magnetometry measurements. In our setup the combination of *p*-polarized incident light in Kerr experiments and the simultaneous detection of the two orthogonal components of the reflected light allow the simultaneous determination of the components of the in-plane magnetization, parallel ($M_{\parallel}$) and perpendicular ($M_{\perp}$) to the field direction.[18] $M_{\parallel}$ originates from the difference of the two components of the reflected light, i.e., Kerr rotation, where as $M_{\perp}$ originates from the small variation of their sum, i.e., reflectivity changes. In-plane resolved hysteresis loops were obtained by averaging many successive iterations, with an acquisition time of 0.25 s/sweep.

The sample is mounted in a stepper motorized eucentric goniometer head, which fixes the plane of reflection for the whole measurements performed. In magneto-optical measurements this is important to be able to compare the values of the magnetization components measured at different angles and between different samples. The study of the magnetization reversal processes and magnetic anisotropy of the films was performed at room temperature by measuring the in-plane resolved *M-H* hysteresis loops as a function of the in-plane angular rotation θ the whole angular range every 1.8°, with 0.5° angular resolution.

For each angle, the experimental hysteresis loops presented here are the result of two consecutive measurements with rotation of the sample by 180° and with the external field with reversed direction. This procedure leads to cancel possible both polar signals coming from an out-of-plane canting of the magnetization,[19] i.e., applied field missalignement, as well as second order terms in the Kerr signal,[20] which are much more important in thin films with in-plane anisotropy.[20] Both contributions are even functions and are easily to cancel, to get just the first order in-plane Kerr signal (odd function), just via subtraction of the two measurements performed with reversed field directions and opposite sample orientations.[21,22] Diamagnetic contributions are compensated via subtraction of a linear, but fixed, function. The fixed slope we have used to correct this diamagnetic contribution in the whole angular range was as small as 1.4% of M_S.

The importance of measuring the in-plane resolved *M-H* hysteresis loops can be emphasize by looking at the loops. The characteristic anisotropy axis directions, i.e., easy and hard axes, and the reversal processes can be determined directly by a simple inspection of the loops. For instance, Fig. 2 shows different magnetization reversal pathways, depending on the α angle. Interestingly, this is more obvious for the $M_{\perp}$ loop. In general, one or two irreversible (sharp) and fully reversible (smooth) transitions are found in both $M_{\parallel}$ and $M_{\perp}$ components. Additionally, depending on which side of the anisotropy directions, i.e., easy and hard axes, the field is applied the magnetization rotates in plane in a clockwise or anticlockwise sense. The sign of the perpendicular component $M_{\perp}$ changes around the easy- and hard-axis directions, when the characteristic directions are crossed. Therefore, $M_{\perp}(H)$ loops are used to locate precisely the characteristic magnetic anisotropy axes, i.e., easy- and hard-axis directions.

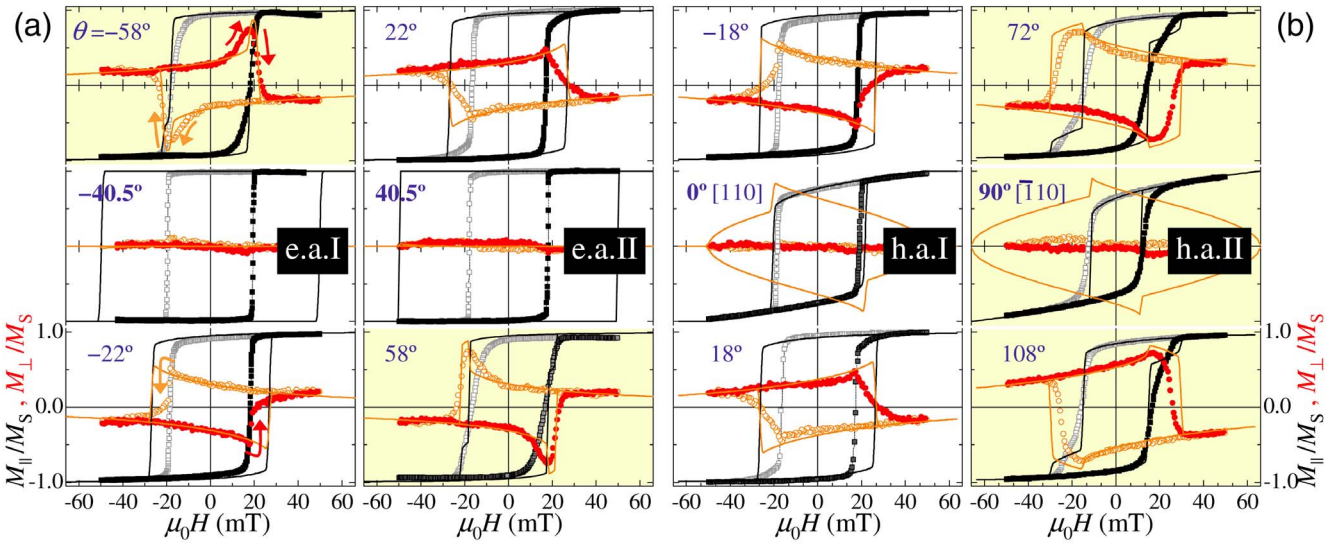

FIG. 2. (Color online) Magnetization reversal study of a 100 ML thick γ'-$Fe_4N(100)$ film around the two *easy axes* (a) and around the two *hard axes* (b) of magnetization. The corresponding applied field angles θ are indicated in the graphs. The experimental $M_{\parallel}(H)$ and $M_{\perp}(H)$ loops are given by squares and circles, respectively. The two branches of the hysteresis are depicted with filled and empty symbols for increasing and decreasing fields, respectively. The lines are the corresponding simulated loops using the model described in the text. Highlighted graphs emphasize reversal governed by two irreversible transitions.

III. RESULTS AND DISCUSSION

Representative Kerr hysteresis loops recorded at selected angles θ between the magnetic field and the crystallographic axes are shown in Fig. 2, in particular, around the easy and hard axes of magnetization. $\theta=0°$ is taken when the external field is aligned parallel to the [110] in-plane crystal direction. Both easy and hard axes are located precisely by looking for the change of sign of the $M_{\perp}(H)$ loops when these characteristic directions are crossed. The middle graphs of Fig. 2(a) show two easy axes slightly displaced with respect to the ⟨100⟩ crystal directions [−40.5° (e.a.I) and +40.5° (e.a.II)].[23] The easy axes are thus not orthogonal to each other, as was found in epitaxial magnetic semiconductors compounds with broken symmetry,[11] but they form an angle $\alpha=81°$. On the contrary, the hard axes are mutually orthogonal [see central graphs of Fig. 2(b)] at 0° (h.a.I) and 90° (h.a.II), i.e., along the [110] and [$\bar{1}$10] crystal directions, respectively.

The shape of the hysteresis loops shows that the magnetization reversal behavior is not consistent simply with the crystalline cubic structure of the film. In a cubic thin film the reversal proceeds with one (two) irreversible transition, related to nucleation and propagation of 180° (90°) domain walls, when the applied field direction is close to one of the two easy- (hard-) axis orientations of magnetization.[24,25] In our films, the two easy-axis loops displayed in the central graphs of Fig. 2(a) are similar, but the behavior of the reversal is *nonsymmetric* for positive and negative angles around the easy axes. For instance, for $\theta=-58°$, i.e., below e.a.I, the $M_{\perp}(H)$ loop presents two transitions (denoted by arrows), whereas only one transition is present above it, e.g., at $\theta=-22°$. The opposite case is found around e.a.II, i.e., one (two) transition for applied field angles below (above) e.a.II. In turn, the hard axis $M_{\parallel}(H)$ loops for $\theta=0°$ and 90° are clearly different in the squareness of the loop as well as in the coercive field [see central graphs of Fig. 2(b)]. The remanence and coercive field values are smaller in h.a.II. Additionally, a different reversal behavior is observed between the two hard axes. Around h.a.II two transitions are clearly observed in the $M_{\perp}(H)$ loops, against only one around h.a.I.

This nonsymmetric reversal behavior is more clear when the angular evolution of the reduced remanences, i.e., $M_{\parallel,R}/M_S$ and $M_{\perp,R}/M_S$, is plotted (Fig. 3). In principle, cubic-symmetry systems should display fourfold symmetry, i.e., a behavior repeated every 90°. In our case, two different behaviors are observed every 180°, which are represented by two differently shaded areas in Fig. 3(a). The symmetry breaking is also reflected in the polar plot of the remanence shown in Fig. 3(b). A butterfly shape is found, instead of the characteristic "four leaves clover" expected from the biaxial anisotropy due to the cubic symmetry of the film.

To gain further insight into the observed features we performed numerical simulations based on a coherent rotation model which includes fourfold K_2(biaxial) and twofold K_1 (uniaxial) anisotropy contributions (see Appendix). K_1 is taken with its easy axis along the [110] crystal direction, i.e., aligned with one of the hard axes of the biaxial anisotropy, according to the morphological characterization. In an external field H, the total energy reads

$$E_{\text{tot}} = K_1 \sin^2 \varphi + \tfrac{1}{4}K_2 \cos^2 2\varphi - \mu_0 M_S H \cos(\theta - \varphi), \quad (1)$$

where M_S is the saturation magnetization, and φ and θ are the angles between the magnetization and the applied field and the [110] crystal direction, respectively. Hysteresis loops are determined numerically via energy minimization of Eq. (1). The experimental data are well reproduced by a value $K_1/K_2=0.15$, which has been obtained by fitting the hard-

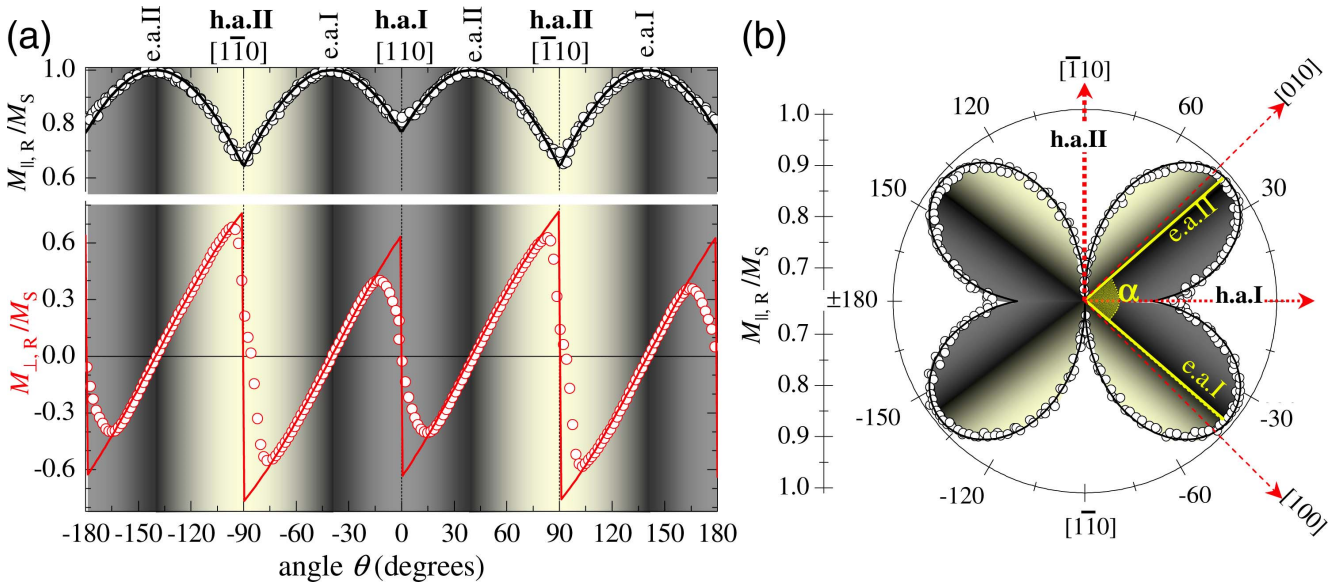

FIG. 3. (Color online) (a) Angular dependence of the reduced remanence $M_{\parallel,R}$ (top graph) and $M_{\perp,R}$ (bottom) as a function of the applied field angle θ for a 100 ML thick γ'-Fe_4N(100) film. The lines are the simulation of the experimental data (symbols) using the model described in the text. The range of angles where different reversal behaviors are found are marked with different shaded areas, e.g., brighter areas indicates the angles where the reversal proceeds by two irreversible transitions (around h.a.II). (b) Polar plot of $M_{\parallel,R}$. Notice that the broken symmetry results in a characteristic butterfly shape behavior of the remanence with nonorthogonal easy axis, but at an angle $\alpha=81°$.

axis hysteresis loops (see bellow). For instance, around the easy axes, the model reproduces qualitatively the shape of both $M_{\parallel}(H)$ and $M_{\perp}(H)$ hysteresis loops, including the nonsymmetric reversal behavior, although the coercivity is overestimated [see Fig. 2(a)]. This is consistent with the behavior expected for a thin film, where the sharp irreversible transitions proceed by propagation of magnetic domains, nucleated in sites with lower anisotropy and/or slightly different orientation, instead of coherent switching as the model assumes. Around the hard axes, i.e., where reversal by rotation is more relevant, both the shape of the reversal and the field transitions are well reproduced with the model [see Fig. 2(b)]. Only h.a.I and h.a.II $M_{\perp}(H)$ loops are not reproduced in the simulation. In the experiment, the signal is averaged over many hysteresis loops and the existence of two equivalent easy axes (inducing magnetization rotation in one way or in the opposite one) cancels $M_{\perp}$. Finally, this simple model reproduces satisfactorily the angular dependence of the reduced remanence components, as shown in Fig. 3.

Additionally, the anisotropy energies involved in the system have been quantified from the hard-axis hysteresis loops by fitting the experimental curves in the neighborhood of $H=0$, as is described in the Appendix. From our experimental data, we extract an anisotropy ratio $K_1/K_2=0.15\pm0.02$ from the magnetization remanence values. From the slopes (see Fig. 6) and taking into account the saturation magnetization value of γ'-Fe_4N $\mu_0 M_S=1.8$ T,[25,26] the estimated fourfold anisotropy is $K_2=(4.5\pm0.3)\times10^4$ J/m^3. It is worth comparing this value to that reported for γ'-Fe_4N prepared by reactive sputtering on $SrTiO_3$ substrates, 1.6×10^4 J/m^3,[26] or prepared by molecular beam epitaxy on MgO(001), 2.9×10^4 J/m^3.[25] The anisotropy constant in our films is closer to that of pure bcc iron (4.8×10^4 J/m^3), which can be an indication of higher crystalline quality.

Some general consequences can be extracted from our results. Within the model it is possible to calculate the angle between the easy axes α as a function of the anisotropy ratio K_1/K_2,[11] as described in the Appendix. The energy minimum is given by

$$\alpha = \arccos \frac{K_1}{K_2}. \tag{2}$$

Consequently, orthogonal easy axes, i.e., $\alpha=90°$, can only be found if $K_1\equiv0$, while the hard axes are always orthogonal, in agreement with the experiment. Figure 4(a) shows that there is an excellent agreement between Eq. (2) and the values extracted from the angular dependence reported for other symmetry breaking epitaxial cubic systems, including metals,[9,10] semiconductors,[11] and insulating[14] magnetic materials. Therefore, the anisotropy balance determines the angle between the easy axes independently of the system. Moreover, it is not even necessary to change the system; it is sufficient to change temperature to observe that the competition between anisotropies determines the angle between easy axes.[11]

Figure 4(b) shows the angular dependence of the reduced remanence components calculated with the model for several anisotropy ratios. The top graph displays the evolution of the parallel component. For increasing K_1/K_2 values, the maximum value of $M_{\parallel,R}/M_S$ (which gives the easy axis) moves toward 0°, breaking the orthogonality of the easy axes, and the remanence at the two hard axes becomes increasingly different. The former is difficult to detect experimentally due

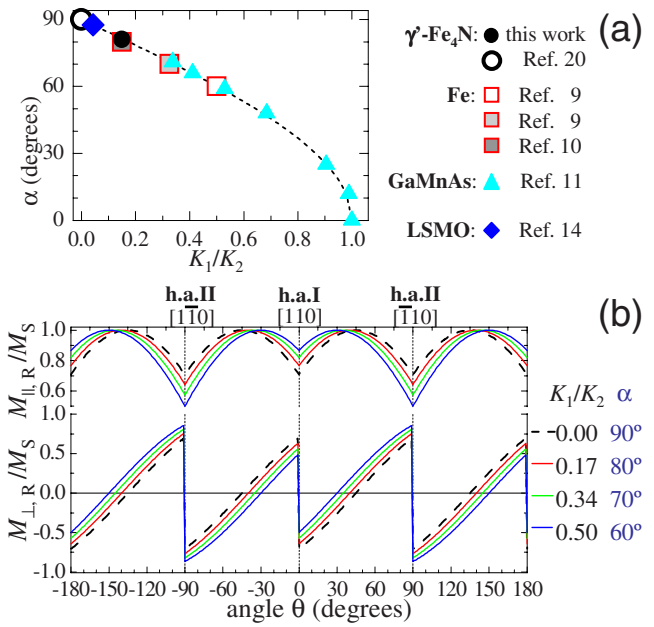

FIG. 4. (Color online) (a) Dependence of the angle between the easy axes α with the anisotropy ratio K_1/K_2. The dashed line is given by Eq. (2). The symbols are extracted from angular dependence studies performed in other symmetry breaking systems. (b) Calculated reduced remanence magnetization components as a function of the angle for the indicated anisotropy ratios. The corresponding α angles are also indicated.

to the sinusoidal behavior of $M_{\parallel,R}/M_S$ around the easy axes. This might explain why the nonorthogonality of the easy axes has not been noticed in experimental studies where only $M_{\parallel}$ is measured. In fact, nonorthogonal easy axes have been resolved only in epitaxial magnetic semiconductor compounds by means of magnetic imaging techniques.[11]

The difference between the remanence values at the hard axes is, however, easier to observe and, in fact, can be found for several other epitaxial cubic symmetry breaking systems where hard-axis hysteresis loops are shown.[6–8,11–16] It has to be noted that the anisotropy ratio, and consequently the angle α between easy axes by using Eq. (2), can be estimated from the remanence values of the parallel component at both hard axes [Eq. (A4) in the Appendix]. In turn, the perpendicular component $M_{\perp,R}/M_S$ is also affected by the symmetry breaking [see bottom graph of Fig. 4(b)]. For increasing K_1/K_2 values, the zero crossing at the easy axes shifts toward 0° and the remanence at the two hard axes becomes increasingly different. Both are easy to observe experimentally, and the zero crossing provides the direct measurement of the angle between easy axes.

Finally, we want to stress that the peculiar magnetization reversal behaviors found in our system, i.e., nonsymmetric reversal around the easy-axis directions and different hard-axis reversal pathways, should take place in the other symmetry breaking epitaxial cubic systems.

IV. SUMMARY

We have studied the symmetry breaking effects on the magnetization reversal properties of epitaxial γ'-$Fe_4N(100)$ systems by vectorial Kerr magnetometry and numerical simulations. Nonsymmetric magnetization reversal and nonorthogonal easy axes have been found to be the main consequences of the broken symmetry, which also result in a characteristic butterfly-shaped polar plot of the remanence. Numerical simulations based on a simple model have been used to address all the aforementioned features. These features depend on additional terms of the magnetic anisotropy. For instance, the competition between the biaxial (fourfold) anisotropy and the additional uniaxial (twofold) anisotropy is the key parameter which controls these effects. On the basis of anisotropy balance, we have shown that the model is applicable to a variety of other symmetry breaking systems, including other metals, semiconductors, and insulating magnetic materials, indicating why many of these effects were not reported before. Simply, the angle between the easy axes and the reversal asymmetry depend on the two anisotropy constants. The anisotropy constants (and thus the ratio between them) can be changed, for example, if another substrate, layer thickness, material, or temperature are employed. This fundamental understanding could be applicable in order to prepare magnetic materials with custom-chosen properties.

ACKNOWLEDGMENTS

J.C. acknowledges support through a "Ramón y Cajal" contract from the Spanish Ministry of Education and Science (MEC). This research was supported by the Comunidad Autónoma de Madrid through Projects GR/MAT/0153/2004 and Nanomagnet S-0505/MAT/0194 and by the MEC through Projects MAT2006-13470 and CSD2007-00010. J.C. and J.V. acknowledge financial support for personnel exchange by the Acciones Integradas Programme, through Grant No. HF2007-0071.

APPENDIX: MODEL DESCRIPTION

Our model is based on the Stoner-Wohlfarth model,[27] including twofold K_1 (uniaxial) and fourfold K_2(biaxial) anisotropy contributions (see Fig. 5). We restrict the system to $K_2 > |K_1| > 0$, as a special case of the general examination

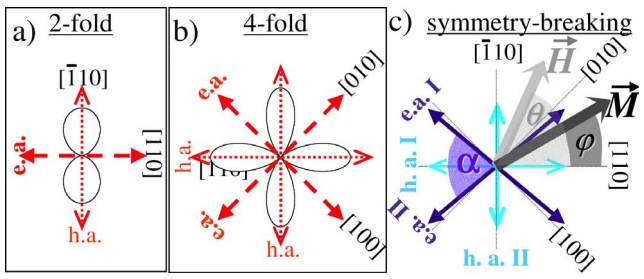

FIG. 5. (Color online) Twofold (uniaxial) (a) and four-fold (biaxial) (b) anisotropy energy surfaces employed in the model. The corresponding easy-axis and hard-axis directions are represented by dashed and dotted lines, respectively. (c) Scheme of the geometry and definition of the angles used in Eq. (1). Note that the broken symmetry results in nonorthogonal easy axes, i.e., $\alpha \neq 90°$.

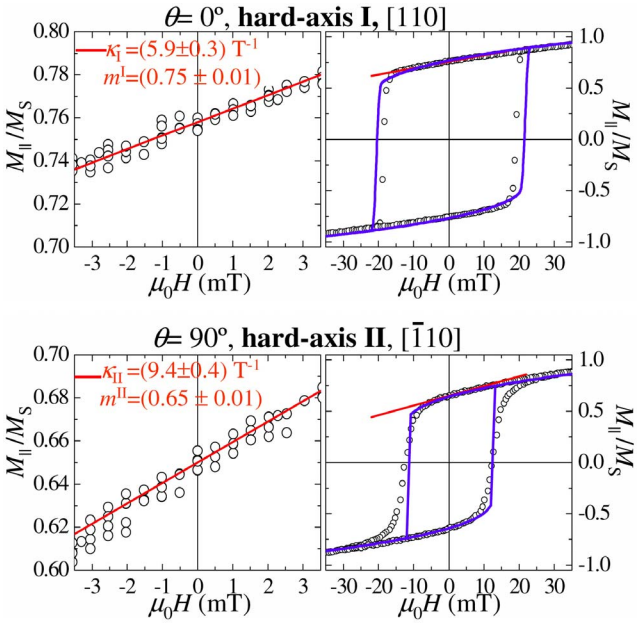

FIG. 6. (Color online) Hard-axis $M_{\parallel}$ hysteresis loops of the symmetry breaking system presented in the paper. The symbols are the experimental data. The left graphs are zoom in to clearly see the fit of the hard-axis loops in the neighborhood of $H=0$. The slopes are given in $1/T$, then μ_0 has to be removed from Eq. (A5). From both slopes and remanence values we extract $K_2=(4.5\pm0.3)\times10^4$ J/m^3 and $K_1/K_2=0.15\pm0.02$. These values are used to calculated the magnetization curves, as described in Appendix 1, depicted with blue lines in the right graphs.

made in Ref. 28. Depending on the sign of K_1 one of the two hard axes of the fourfold anisotropy changes. Changing the sign virtually rotates the system by $\pi/2$, leaving the physics unchanged. Thus, only $K_1 \geqslant 0$ has to be considered. The total energy of the system E_{tot} is, thus, given by Eq. (1) as follows:

$$E_{\text{tot}} = K_1 \sin^2\varphi + \tfrac{1}{4}K_2 \cos^2 2\varphi - \mu_0 M_S H \cos(\theta-\varphi),$$

where M_S is the saturation magnetization, H is the applied field, and φ and θ are the angles between the magnetization and the applied field and the [110] crystal direction, respectively [see Fig. 5(c)]. For $K_1 \geqslant K_2$ the system becomes truly uniaxial with only one easy axis.

1. Magnetization components

In the model the magnetization follows the local energy minimum via coherent rotation. For each applied field angle θ the magnetization hysteresis loops are determined numerically via energy minimization of Eq. (1) as follows:

$$\frac{\partial E_{\text{tot}}(H)}{\partial\varphi} = 0. \tag{A1}$$

The magnetization components are then derived by using

$$M_{\parallel}(H)/M_S = \cos(\theta-\varphi),$$

$$M_{\perp}(H)/M_S = \sin(\theta-\varphi). \tag{A2}$$

2. Anisotropy-dependent angle between easy axes

With this simple model it is possible to determine the dependence of the angle between easy-axis α with the anisotropy ratio K_1/K_2. If $\theta=0°$ or $\theta=90°$, i.e., the hard-axis directions, it is possible to cancel either sin φ or cos φ from the explicit expression of Eq. (A1). Assuming that both are nonzero for small fields, Eq. (A1) can be reduced to to a third order equation in cos φ or sin φ, respectively. This third order equation has three exact real solutions for $H < \sqrt{8/27}\sqrt{(K_2 \pm K_1)^3/K_2}$, where the plus and minus sign refers to $\theta=0°$ and $\theta=90°$, respectively. If $H=0$, the solution for the equilibrium α angle is straightforward as the constant term of the third order equation is zero. The first of the three solutions represents one energy maximum. The result for the minima is Eq. (2),

$$\alpha = \arccos\frac{K_1}{K_2}.$$

Consequently, orthogonal easy axes, i.e., $\alpha=90°$, are only found if $K_1 \equiv 0$, while the hard axes are always orthogonal. By inversion of Eq. (2) it is possible to determine K_1/K_2 from the angle between the two easy axes.

3. Quantifying anisotropies

The anisotropy energies involved in the system can be quantified from the hard-axis hysteresis loops by fitting the experimental curves in the neighborhood of $H=0$. For instance, it is possible to minimize the energy [Eq. (1)] in a hard-axis direction for a nonzero field H. A Taylor series with respect to H in the vicinity of $H=0$ provides[29]

$$\left.\frac{M_{\parallel}}{M_S}\right|_{H\approx0} = \sqrt{\frac{1 \pm \frac{K_1}{K_2}}{2} + \frac{\mu_0 M_S}{4(K_2 \pm K_1)}H}, \tag{A3}$$

where the $(+)$ corresponds to the hard-axis I, i.e., the fourfold hard axis which coincides with the easy-axis direction of the twofold anisotropy, while the $(-)$ corresponds to the hard-axis II, i.e., the common fourfold and twofold hard axes [see Fig. 5]. Therefore, it is also possible to calculate K_1/K_2 from either the reduced remanence values of the parallel component at the hard axes, i.e., $m^{\text{I}}=\frac{M^{\text{I}}_{\parallel,\text{R}}}{M_S}$ and $m^{\text{II}}=\frac{M^{\text{II}}_{\parallel,\text{R}}}{M_S}$ as follows:

$$K_1/K_2 = (m^{\text{I}})^2 - (m^{\text{II}})^2, \tag{A4}$$

while the two slopes of the hard-axis loops at $H=0$, κ_{I} and κ_{II}, enable the separation of K_1 and K_2 as follows:

$$K_1 = \frac{\mu_0 M_S}{8}\left(\frac{1}{\kappa_{\text{I}}} - \frac{1}{\kappa_{\text{II}}}\right),$$

$$K_2 = \frac{\mu_0 M_S}{8}\left(\frac{1}{\kappa_{\text{I}}} + \frac{1}{\kappa_{\text{II}}}\right). \tag{A5}$$

The error in fitting K_1 and K_2 (calculated from the inverse of relatively small slopes) can be minimized by including the knowledge of K_1/K_2, derived from the angle between easy axes, into the fit by using Eq. (2).

*Present address: Institut für Angewandte Physik, Universität Hamburg, 20355 Hamburg, Germany.
†Author to whom correspondence should be addressed; julio.camarero@uam.es

[1] S. D. Bader, Rev. Mod. Phys. **78**, 1 (2006).
[2] J. J. de Miguel and R. Miranda, J. Phys.: Condens. Matter **14**, R1063 (2002).
[3] G. Bertotti, *Hysteresis in Magnetism* (Academic, New York, 1998).
[4] F. J. Himpsel, J. E. Ortega, G. J. Mankey, and R. F. Willis, Adv. Phys. **47**, 511 (1998).
[5] D. Weller, J. Stöhr, R. Nakajima, A. Carl, M. G. Samant, C. Chappert, R. Megy, P. Beauvillain, P. Veillet, and G. A. Held, Phys. Rev. Lett. **75**, 3752 (1995).
[6] R. K. Kawakami, E. J. Escorcia-Aparicio, and Z. Q. Qiu, Phys. Rev. Lett. **77**, 2570 (1996).
[7] Y. B. Xu, D. J. Freeland, M. Tselepi, and J. A. C. Bland, Phys. Rev. B **62**, 1167 (2000).
[8] O. Thomas, Q. Shen, P. Schieffer, N. Tournerie, and B. Lépine, Phys. Rev. Lett. **90**, 017205 (2003).
[9] Y. Zhai, L. Shi, W. Zhang, Y. X. Xu, M. Lu, H. R. Zhai, W. X. Tang, X. F. Jin, Y. B. Xu, and J. A. C. Bland, J. Appl. Phys. **93**, 7622 (2003).
[10] R. Żuberek, K. Fronc, W. Paszkowicz, and H. Szymczak, J. Magn. Magn. Mater. **283**, 28 (2004).
[11] U. Welp, V. K. Vlasko-Vlasov, X. Liu, J. K. Furdyna, and T. Wojtowicz, Phys. Rev. Lett. **90**, 167206 (2003).
[12] K.-Y. Wang, M. Sawicki, K. W. Edmonds, R. P. Campion, S. Maat, C. T. Foxon, B. L. Gallagher, and T. Dietl, Phys. Rev. Lett. **95**, 217204 (2005).
[13] X. Liu and J. K. Furdyna, J. Phys.: Condens. Matter **18**, R245 (2006).
[14] M. Mathews, F. M. Postma, J. C. Lodder, R. Jansen, G. Rijnders, and D. H. A. Blanka, Appl. Phys. Lett. **87**, 242507 (2005).
[15] S. van Dijken, G. Di Santo, and B. Poelsema, Phys. Rev. B **63**, 104431 (2001).
[16] F. Bisio, R. Moroni, F. Buatier de Mongeot, M. Canepa, and L. Mattera, Phys. Rev. Lett. **96**, 057204 (2006).
[17] J. M. Gallego, S. Yu. Grachev, D. M. Borsa, D. O. Boerma, D. Ecija, and R. Miranda, Phys. Rev. B **70**, 115417 (2004).
[18] J. Camarero, J. Sort, A. Hoffmann, J. M. García-Martín, B. Dieny, R. Miranda, and J. Nogués, Phys. Rev. Lett. **95**, 057204 (2005).
[19] H. F. Ding, S. Pütter, H. P. Oepen, and J. Kirschner, J. Magn. Magn. Mater. **212**, L5 (2000).
[20] R. M. Osgood III, B. M. Clemens, and R. L. White, Phys. Rev. B **55**, 8990 (1997).
[21] H. F. Ding, S. Pütter, H. P. Oepen, and J. Kirschner, Phys. Rev. B **63**, 134425 (2001).
[22] T. Mewes, H. Nembach, M. Rickart, and B. Hillebrands, J. Appl. Phys. **95**, 5324 (2004).
[23] D. Ecija, E. Jiménez, J. Camarero, J. M. Gallego, J. Vogel, N. Mikuszeit, N. Sacristán, and R. Miranda, J. Magn. Magn. Mater. **316**, 321 (2007).
[24] E. Gu, J. A. C. Bland, C. Daboo, M. Gester, L. M. Brown, R. Ploessl, and J. N. Chapman, Phys. Rev. B **51**, 3596 (1995).
[25] J. L. Costa-Krämer, D. M. Borsa, J. M. García-Martín, M. S. Martín-González, D. O. Boerma, and F. Briones, Phys. Rev. B **69**, 144402 (2004).
[26] K. R. Nikolaev, I. N. Krivorotov, E. D. Dahlberg, V. A. Vas'ko, S. Urazhdin, R. Loloee, and W. P. Pratt, Appl. Phys. Lett. **82**, 4534 (2003).
[27] E. C. Stoner and E. P. Wohlfarth, Philos. Trans. R. Soc. London, Ser. A **240**, 599 (1948).
[28] Y. T. Millev, H. P. Oepen, and J. Kirschner, Phys. Rev. B **57**, 5837 (1998).
[29] Usually, the magnetization curves are fitted by applying a fit to a third order polynomial, i.e., in hard-axis direction, the field is a third order function of the magnetization. This is easily seen by combining Eqs. (1) and (A2), and additionally fulfilling Eq. (A1). A fit therefore requires a transformation of the data, i.e., an interchange of x and y as well as the removal of the data in the unphysical regions of the polynomial. Instead we solve the third order equation giving three functions $M(H)$; two for the upper and lower branches and one for the unphysical switching region. Picking the right solution and making a Taylor expansion of the two inverted polynomials (one for each hard axis) give the solution in Eq. (A3).